IEEE Photonics Journal
An IEEE Photonics Society Publication

Open Access

Free Space Vortex Light by Diffraction of a Bessel Beam From Optical Fiber

Volume 9, Number 4, August 2017

Hang Ruan
Liang Wang
Shengnan Wu
Liu liu
Bin Zhou

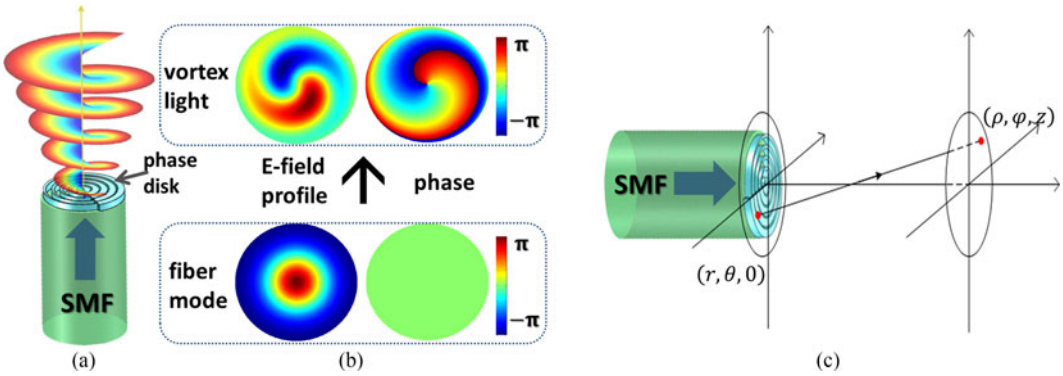

DOI: 10.1109/JPHOT.2017.2723437
1943-0655

IEEE photonics SOCIETY

IEEE

Free Space Vortex Light by Diffraction of a Bessel Beam From Optical Fiber

Hang Ruan,[1,†] Liang Wang,[2,†] Shengnan Wu,[3] Liu liu,[1] and Bin Zhou[1]

[1]South China Academy of Advanced Opto- Electronics, South China Normal University, Guangzhou 510631, China
[2]Department of Electronic Engineering, The Chinese University of Hong Kong, Shatin Hong Kong
[3]Centre for Optical and Electromagnetic Research, State Key Laboratory of Modern Optical Instrumentation, Zhejiang Provincial Key Laboratory for Sensing Technologies, Zhejiang University, Hangzhou 310058, China

DOI:10.1109/JPHOT.2017.2723437

Manuscript received May 19, 2017; revised June 21, 2017; accepted June 30, 2017. Date of publication July 4, 2017; date of current version July 13, 2017. This work was supported in part by the National Natural Science Foundation of China under Grant 61307053, in part by the China Post-Doctoral Science Foundation under Grant 2016M590794, and in part by the the Joint International Research Laboratory of Optical Information. Hang Ruan† and Liang Wang† contributed equally to this work. Corresponding author: Bin Zhou (e-mail: zhoubin_mail@163.com).

Abstract: A free space vortex light generator is designed based on the diffraction of an optical Bessel beam. The Bessel beam propagating in a single mode fiber is modulated by a helical phase disk designed at the fiber end and gradually evolves to vortex light in free space. The properties of the generator such as operation wavelength range, polarization sensitivity, and fabrication tolerance are analyzed using finite-difference time-domain software. With the inherent advantage of the "nondiffraction" feature of the Bessel beam naturally obtained from an optical fiber, the proposed fiber vortex light generator would have potential applications in high-resolution imaging, particle trapping, manipulation, and so on.

Index Terms: Advanced optics design, diffractive optics, subwavelength structures.

1. Introduction

Vortex light, also known as photonic quantum vortex, is the light twisting like a corkscrew around its axis [1]–[5]. Research on the properties of light vortices has thrived since the publication of a paper by John Nye and Michael Berry in 1974, describing the basic properties of "dislocations in wave trains" [2]. One of the most important parameter of a vortex light is the topological charge which can be an integer or fraction, with positive or negative sign depending on the direction of the light twist [3], [4]. The number of the topological charge describes how many twists the light does in one wavelength [1], [4]. The higher the number of the topological charge is, the faster the light spins around the axis. Vortex light carries Orbital Angular Momentums (OAM) [4] and has attracted great attention due to its potential applications in super resolution imaging [5]–[7], particle manipulation [8], [9], high capacity optical communication [10]–[13] and quantum computing [14], [15]. For example, in optical microscopy, to enhance the spatial resolution, the vortex light with donut like intensity distribution has been employed to deplete the fluorophores around the observation area so as to shrink the area of the fluorescence excited by a Gaussian beam at another wavelength [5]. Also with the donut like intensity profile the vortex light has been applied to trap micro- and

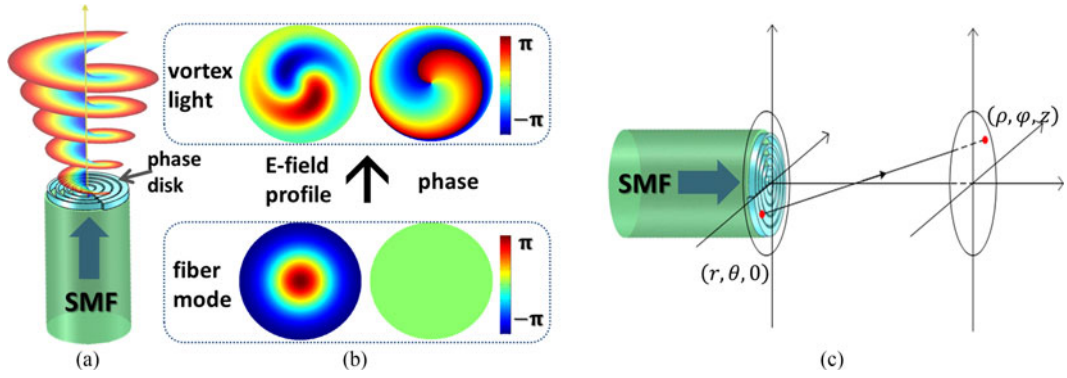

Fig. 1. Principle of the fiber-based free space vortex light generator. (a) Structure of the fiber-based vortex light generator; (b) electrical field and phase distributions before and after the fundamental HE_{11} mode passes through the phase disk to free space; (c) illustration of the diffraction of the Bessel beam after passing through the phase disk.

nano- particles at its high intensity ring, and by its angular momentum the small particles have been rotated [8], [9]. Moreover, vortex light helps improve the capacity of the optical communication from a new degree of freedom which is beyond conventional multiplexing techniques, e.g. 2.4 Tbit/s per wavelength channel and 2.5 Tbit/s per wavelength channel have been reported soon after the use of the OAM in optical communication link [16].

On the other hand, due to "non-diffraction" feature the Bessel beams and quasi-Bessel beams have attracted lots of attentions [17]–[21] and also have been used in high resolution imaging with similar operation principle to the vortex light [6], [7]. In particle trapping and atomic optics, the non-diffraction feature of the Bessel beams confines the particle in a tunnel whose diameter does not varies along the beam propagation direction [17], [22]. Based on multi-ring structure the ability to confine both high and low refractive index particles using a Bessel beam is possible [23]–[25]. Low index particles are confined in the dark rings while high index particles are confined in the bright rings, which cannot be achieved with Gaussian beams.

The vortex light and Bessel beam have their own unique advantages and vortex light generated from Bessel beam would inherently possesses both the advantages, and could attract great interest. Light sources with Bessel beam profile are commonly generated using diffractive optics [17], spatial light modulators (SLM) [26], transmissive axicons [27], holographic techniques [28], and so on. In this paper, we present a new way of generating the free space vortex light by diffraction of a Bessel beam inside an optical single mode fiber with a helical phase disk designed at the fiber end. Previously we have used similar phase disk structure to convert optical fiber LP mode to OAM mode propagating in few mode fiber [30], while in this work we demonstrate the converted vortex light has unique properties when propagating in free space. As optical light confined in the single mode fiber is natural Bessel beam, many complicated free space optical components to generate the Bessel beams can be avoided. And our scheme does not need optical components for the light beam alignment, splitting, focusing etc which are required in free space optics to adjust the complicated optical path. Moreover, the fiber based vortex light generator is stable compared with that by free space optics where any minor change of a component will affect the overall performance of the system.

2. Principle and Design of the Fiber-Based Free Space Vortex Light Generator

The proposed free space vortex light generator is made at a single mode fiber (SMF) end by fabricating a phase disk which is made up of many coaxial rings, as shown in Fig. 1(a). The width of the rings increases linearly together with the azimuth angle and the maximum width is designed to be smaller than the operating wavelength according to the effective medium theory. Therefore, the

effective refractive index at the SMF end will change linearly with azimuth angle [29]. The wavefront of the transmitted light is modulated by the phase disk so as to covert the fundamental fiber mode HE_{11} to the free space vortex light, as shown in Fig. 1(b). Quasi-diffractionless free space vortex light is thus generated at the end of SMF. This vortex light generation process can be viewed as diffraction of a Bessel beam in SMF when it is passing through the phase disk, as shown in Fig. 1(c). Note that we use "quasi-diffractionless" to describe the vortex light generated from Bessel beam since the diffraction of Bessel beam is much smaller than that of other types of beams. Actually the ideal zeroth-order Bessel beam is diffractionless when it is of infinite transverse extent and carries infinite amount of energy [32].

In a circular symmetrical step-index optical fiber, the fiber modes are described with different orders of Bessel functions. The electrical field distribution of the fundamental mode, i.e. HE_{11} mode, at fiber cross section (r, θ) is [31]:

$$E_{HE11}\ (r,\theta) = \begin{cases} AJ_0\left(\frac{U}{a}r\right)\ r \le a \\ BK_0\left(\frac{W}{a}r\right)\ r > a \end{cases}, \tag{1}$$

where J_0 is the zero-order Bessel function of the first kind, K_0 is the zero-order modified Bessel function of the second kind, a is the fiber core radius, U and W are dimensionless model parameters, A and B are constants.

To generate the vortex light from HE_{11} mode, a phase disk is introduced at the fiber end. The wavefront of the light passing through the phase disk is linearly modulated along azimuth angle. In order to generate a vortex light with integer number of topological charge, the phase change of total 360° azimuth angle should be an integer number of 2π. So at the output plane of the phase disk, i.e. $z = 0$, the HE_{11} mode is converted to be:

$$E_{votex\_Bessel}\ (r,\theta,0) = \begin{cases} AJ_0\left(\frac{U}{a}r\right)\exp\left(-il\theta\right)\ r \le a \\ BK_0\left(\frac{W}{a}r\right)\exp\left(-il\theta\right)\ r > a \end{cases}, \tag{2}$$

where l is the number of topological charge. The phase disk acts as the device for diffraction and the diffracted field at the location (ρ, φ, z) can be written mathematically in cylindrical coordinate as:

$$\begin{aligned} E_{votex_{Bessel}}(\rho,\varphi,z) &= \frac{-ik}{2\pi z}e^{-ikz}\iint E_{votex\_Bessel}(r,\theta,0)\exp\left[-\frac{ik}{2z}\left(\rho^2 - 2\vec{\rho}\,\vec{r} + r^2\right)\right]rdrd\theta \\ &= -\frac{kAi^{l+1}}{z}e^{-ikz}\exp\left(\frac{-ik}{2z}\rho^2\right)\exp\left(-il\varphi\right)\int_0^\infty J_l\left(\frac{k\rho}{z}r\right)J_0\left(\frac{U}{a}r\right)\exp\left[-\frac{ik}{2z}r^2\right]rdr \end{aligned} \tag{3}$$

The vortex light with topological charge order of one can be obtained when set l with 1. When a linearly polarized light passes through the helical phase disk and propagates to free space, the angular momentum of the light increases and its optical field distribution changes accordingly. With the increase of the propagation distance, the waist radius of the generated vortex light will gradually expand. To show the quasi-diffractionless property of the proposed vortex light generated from Bessel beam, we compare it with the one from Gaussian beam. The vortex beam with topological charge one diffracted from a Gaussian beam can be described as [33]:

$$E_{votex\_Gauss}\ (\rho,\varphi,z) = -\frac{E_0\exp\left[i\left(kz+\varphi\right)\right]\rho}{\left(q\ -\ i\right)^2 w_0}\exp\left[-\frac{\left(1\ -\ iq\right)\rho^2}{\left(1+q^2\right)w_0{}^2}\right] \tag{4}$$

where w_0 is the waist radius and $q = 2z/kw_0{}^2$. When referring to the non-diffraction feature of a Bessel beam, it usually means the size of the dark central core does not change along its propagation direction, which is important in many applications such as high resolution imaging and light tweezers [17]. For comparison the size of the dark central core is defined as the radius where the optical intensity reduces to 1/e of its maximum value of the first bright ring. Based on Eq. 3 and Eq. 4, Fig. 2 plots the size of the dark central core versus propagation distance for the vortex

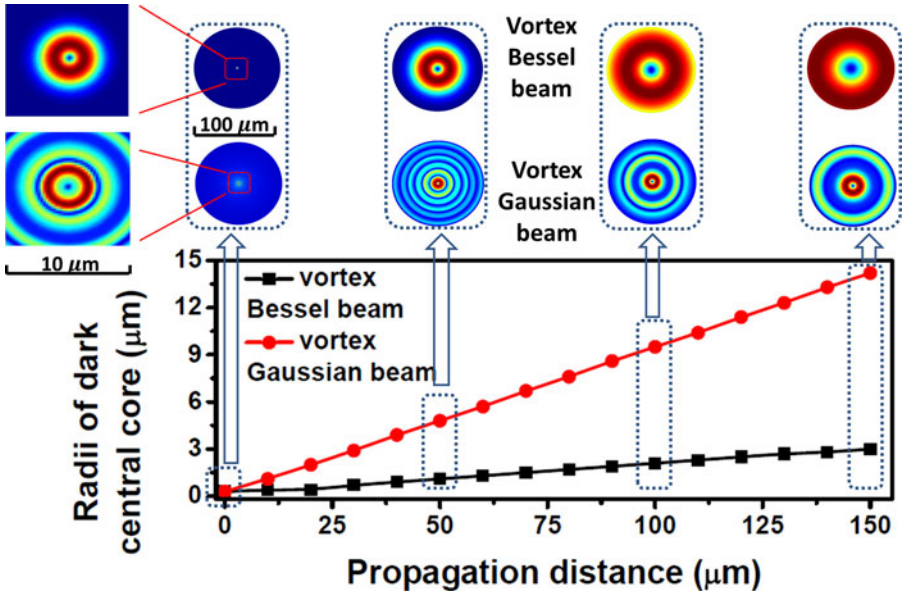

Fig. 2. The variation of the dark central core of the vortex light generated from Gaussian beam and Bessel beam along propagation distance. The optical intensity distribution for the two vortex lights at z = 0 μm, 50 μm, 100 μm and 150 μm are also shown.

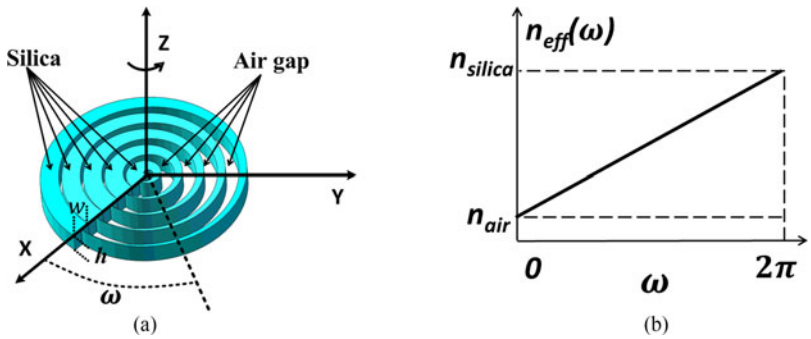

Fig. 3. 3D structure of the phase disk for the proposed vortex light generator. (a) The phase disk formed by many coaxial helical rings with W as the maximum width of each helical ring at $\omega = 0$ and h as the height; (b) effective refractive index of the phase disk varies with the azimuth angle.

light generated form Bessel beam and Gaussian beam, respectively. To give a fair comparison, the waist position and radius of the Gaussian beam are set to be z = 0 and 0.9 μm, which results in the same radius of the dark central core at z = 0 for both the vortex light generated from Bessel and Gaussian beams. We can see from Fig. 2 that the radius of the dark central core at z = 0 is 0.3 μm for both Bessel and Gaussian beams and it increases almost linearly within a short propagation distance. However, the radius of Bessel beam generated vortex light increases remarkably slower compared with that of Gaussian beam generated vortex light. At the propagation distance of 150 μm, the radius for Bessel and Gaussian beams generated vortex light are 3 μm and 14.2 μm respectively, which indicates the quasi-diffractionless property of the generated vortex light by our proposed fiber-based generator.

The phase disk is designed based on the effective medium theory: the effective refractive index of a composite material is the weighted sum of refractive index of the constituents that form the medium [29]. Similar to our previous work [30], the phase disk is made up of many coaxial rings whose width increases linearly with the azimuthal angle, as shown in Fig. 3(a). The material of the rings is chosen to be silica to match with the optical fiber in order to decrease Fresnel reflection.

The gaps between the rings are filled with air. Thus the ratio between silica and air of the phase disk is linearly changing which results in the linear change of effective refractive index along the azimuth angle. The parameters of the rings are given as follows:

$$\begin{cases} R_{inner_m}(\omega) = (m-1)W + \frac{W(2\pi-\omega)}{4\pi} \\ R_{outer_m}(\omega) = mW - \frac{W(2\pi-\omega)}{4\pi} \\ W_m(\omega) = R_{outer_m}(\omega) - R_{inner_m}(\omega) = \frac{W\omega}{2\pi} \\ h = \frac{l\lambda}{n_{silica}-n_{air}} \end{cases}, \tag{5}$$

where ω is the azimuth angle, W is the maximum width of each helical ring at $\omega = 2\pi$ and $W_m(\omega)$ is the width of the m-th ring counted from the center at azimuth angle of ω, $R_{inner_m}(\omega)$ and $R_{outer_m}(\omega)$ are the inner and outer radius of m-th ring, h is the height of each ring, l is the targeting number of topological charge to be achieved, λ is the operating wavelength, n_{silica} and n_{air} are the refractive index of the silica and air, respectively. According to the effective medium theory, the effective refractive index of the helical phase disk at azimuth angle of ω can be expressed as [29]:

$$n_{eff}(\omega) = \sum_m \frac{[n_{silica}W_m(\omega) + n_{air}(W - W_m(\omega))]}{W} = n_{air} + \frac{(n_{silica} - n_{air})\omega}{2\pi} \tag{6}$$

Note that as the polarization of the input light is not known we do not use the linear combination of TE and TM polarizations to calculate the effective refractive index [34]. Instead we use Eq. 6 for the calculation which is verified to be valid in the following result showing polarization-insensitivity of our design. Fig. 3(b) depicts the linear relationship between the effective refractive index of the phase disk and the azimuth angle based on Eq. 6. To generate a vortex light with topological charge order of $l = 1$, the phase difference between the azimuth angle at $\omega = 0^-$ and $\omega = 0^+$ should be 2π, which is realized by controlling the height h in Eq. 5 (0^- and 0^+ means to approach 0 from the negative and positive side, respectively). The height of the phase disk is set to be uniform everywhere to make the fabrication easily.

3. Simulation and Analysis

The performances of the proposed vortex light generator are evaluated through simulation using Lumerical 3D FDTD software. The uniform mesh grid is set to be 0.1 μm in the three dimensional rectangular coordinate system. The diameters of the fiber core and cladding are set to be 10 μm and 25 μm, and the corresponding refractive index are 1.45 and 1.44, respectively. n_{silica} in the phase disk is 1,44. The cladding size is set so as to make sure the simulation region is large enough to get a reasonable result and save the computing memory. The operating wavelength is set at $\lambda = 1550$ nm. The height of the phase disk rings h is 3.523 μm to produce the vortex light with topological charge of 1. According to the effective medium theory, the maximum width W is set to be small enough (0.25 μm unless specified elsewhere) compared to the operating wavelength [29]. The light source in the simulation has a fundamental mode HE_{11} in the optical fiber. As the HE_{11} mode passes though the phase disk and propagates in free space, its wavefront is modulated and then evaluated in free space.

In order to quantitatively evaluate the performance of the proposed vortex light generator, the parameter of beam purity is introduced, which is the correlation coefficient between the vortex light generated by the proposed vortex light generator and the mathematically calculated vortex light based on Eq. (3). Beam purity P_l is given by the following expression:

$$P_l = \frac{\iint \left| \vec{H}_l \times \overrightarrow{E_{votex\_Bessel}} \right| dS}{\sqrt{\iint \left| \vec{E}_l \times \vec{H}_l \right| dS \cdot \iint \left| \overrightarrow{E_{votex\_Bessel}} \times \overrightarrow{H_{votex\_Bessel}} \right| dS}}, \tag{7}$$

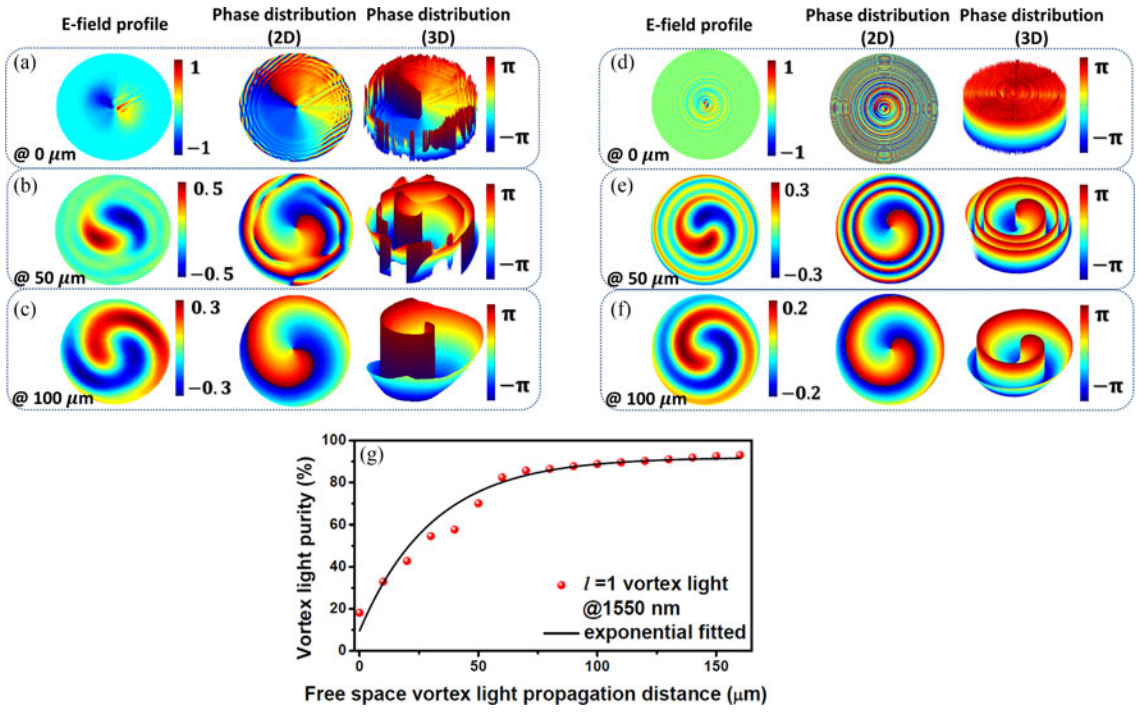

Fig. 4. The evolution of the vortex light propagating in free space. (a)–(c) Evolution of the normalized electrical field profile and phase distribution of the generated vortex light by FDTD simulation for different propagation distance; (d)–(f) evolution of the normalized electrical field profile and phase distribution of the mathematically calculated vortex light for different propagation distance; (g) beam purity versus propagation distance in free space.

where $\overrightarrow{E_{votex\_Bessel}}$ and $\overrightarrow{H_{votex\_Bessel}}$ are the electric and magnetic fields of the mathematically calculated vortex light, and $\vec{E}_l$ and $\vec{H}_l$ are the electric and magnetic fields of the generated vortex light by FDTD simulation using the proposed generator. For simplify, we use the correlation between the electrical fields to replace that of the electromagnetic fields expressed in free space:

$$P_l = \frac{\oint\oint \left| \vec{E}_l \times \overrightarrow{E_{votex\_Bessel}} \right| dS}{\sqrt{\oint\oint \left| \vec{E}_l \right|^2 dS \cdot \oint\oint \left| \overrightarrow{E_{votex\_Bessel}} \right|^2 dS}}, \tag{8}$$

Fig. 4(a)–(f) shows the evolution of electrical field and phase distribution of the vortex light when it is propagating in free space using FDTD simulation and mathematical calculation, respectively. The maximum field intensity at the propagation distance of zero is set to be 1 as reference, and the field intensity is normalized according to this. The size of the subcomponent in the phase disk is designed as small as possible according to effective medium theory, however the size cannot be infinitely small which is limited by memory cost in simulation and the fabrication cost, so the generated vortex light is not perfect. Fig. 4(g) shows the evolution of the purity P_l along the propagation distance in free space. The purity P_l describes how close the simulated vortex light is to the mathematically calculated one. In Fig. 4(g) P_l increases fast within the initial 100 μm distance and reaches nearly 90% and then becomes almost stable. This agrees well with the fact that the Bessel beam has a fascinating ability of reconstruction [35], and thus it can recover to Bessel beam again within a short propagation distance. The purity increases significantly because the undesired beam due to the unsmooth phase disk has larger diffraction angle and would expand faster until out of the simulation region within a short propagation distance. It is worth mentioning that an exponential curve fits well

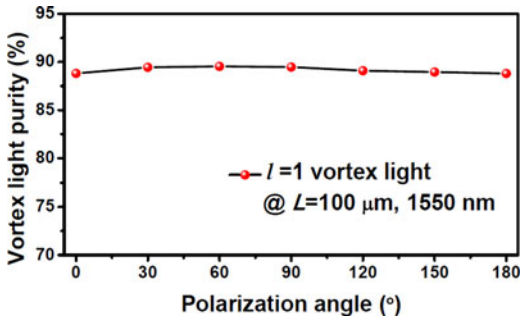

Fig. 5. Purity of the vortex light at a propagation distance of 100 μm in free space versus polarization angle. The polarization angle changes from 0 to π.

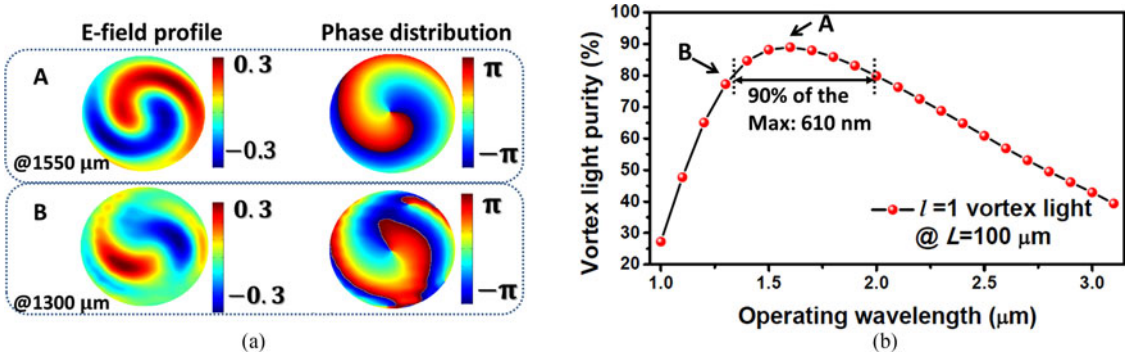

Fig. 6. (a) The normalized electrical field profile and phase distribution of the generated vortex light at two different wavelengths (A: 1300 nm; B: 1550 nm) (b) purity of the vortex light versus operating wavelength where A and B correspond to those in (a). The propagation distance is 100 μm in free space.

the trend of purity growth especially at larger propagation distance. However, we have not got exact theoretical reason to explain the exponential fitting yet, we put this phenomenon in this paper and hope to enlighten the researchers in this field. In the following part of the paper, we choose the field data at the propagation distance of 100 μm for further analysis.

The polarization characteristics of the generator is studied by changing the polarization angle of the HE_{11} mode from 0 to π. The simulation result is shown in Fig. 5. The purity of the generated vortex light with $l = 1$ maintains around 90% at the propagation distance of 100 μm in free space and only has little fluctuation for different polarizations, which implies polarization insensitive property of the proposed generator.

The purity degradation due to the wavelength mismatch is also investigated and the results are shown in Fig. 6. The target operation wavelength is 1550 nm when the height is set to be 3.523 μm for $l = 1$ according to Eq. 5. Fig. 6(a) plots the normalized electrical field profile and the corresponding phase distribution of the generated vortex light at wavelength of 1550 nm (the maximum purity) and 1300 nm (about 90% of the maximum purity), respectively. The deterioration of the vortex light is obvious when the working wavelength deviates from the target value (1550 nm). Thus the deviation from the target operation wavelength leads to a decrease of the purity, as shown in Fig. 6(b). The bandwidth for the purity falling to 90% of the maximum value is 610 nm, which shows a wide working bandwidth for superior performance in many applications.

In fact there would be a certain range of fabrication error during the fabrication process which will affect the purity of the generator. Different height of the phase disk h has been used for simulation to evaluate the fabrication tolerance while other parameters are kept the same as the simulation in Fig. 4. The height tolerance is defined as $\Delta h = (3.523\ \mu\text{m} - h_{act})$, where 3.523 μm is the target value of the disk height and h_{act} is the actual height value used in each simulation. The result is

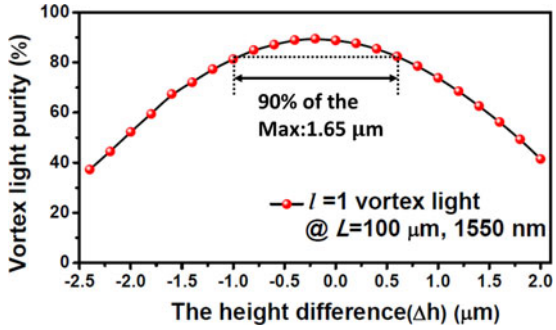

Fig. 7. Purity of the vortex light versus height of the phase disk at a propagation distance of 100 μm in free space.

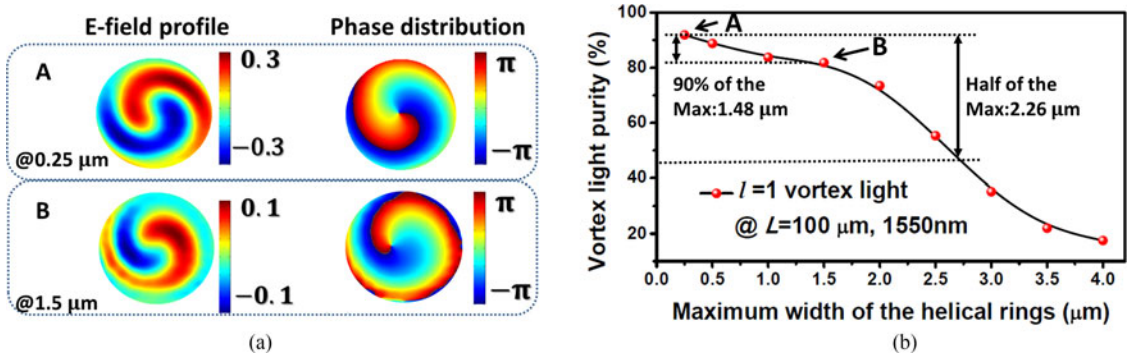

Fig. 8. (a) The normalized electrical field profile and phase distribution of the generated vortex light for two different widths (A: 0.25 μm, B: 1.5 μm); (b) purity of the vortex light versus maximum width of the helical rings. The propagation distance is 100 μm in free space.

given in Fig. 7, indicating that the purity decreases gradually when the height of the helical phase disk deviates from the target value. The range of the height deviation for purity falling to 90% of the maximum value is from -1 μm to 0.65 μm which shows large fabrication tolerance to the height of the phase disk.

In order to satisfy the condition for the effective medium theory, W at azimuth angle $\omega = 2\pi$ is set to be 0.25 μm, which is much smaller than the operating wavelength. However, it results in the challenge on the fabrication due to the small dimension. Here we study the effect of various width values of the helical rings in the phase disk. The normalized electrical field profile and the corresponding phase distribution of the generated vortex light are shown in Fig. 8(a), when the value of W is 0.25 μm (maximum purity) and 1.5 μm (90% of the maximum purity), respectively. When the width is away from the defined value of 0.25 μm, the deterioration of the generated vortex light is clear. By gradually changing the width while fixing the wavelength at 1550 nm and the height at 3.523 μm, we obtain the purity as a function of width shown in Fig. 8(b). As width W gradually increases, the size of the silica rings or the air gap becomes larger than the wavelength, which violates the basic condition of the effective medium theory [29]. Thus the purity decreases as the width increases. In order to keep the high purity, W should be less than 1.5 μm.

For the above results, the target topological order of the structure is 1. However, due to the unsmooth structure, limited mesh grid size and limited simulation region, the purity of the generated vortex light is around 90%, and the remaining 10% consists of vortex light with other orders and various kinds of stray light. Fig. 9(a) shows the proportion of the vortex light with different topological charge orders derived from Eq. 8 when the the target topological order is set to be $\mathrm{l} = 1, 2$ and 3, respectively. Fig. 9(b)–(d) are the normalized electrical field and the phase distribution for the corresponding target topological order. Take the target topological order $\mathrm{l} = 1$ as an example: the intensity proportion of vortex light with order of 1 is at least 73 dB larger than that of intensity

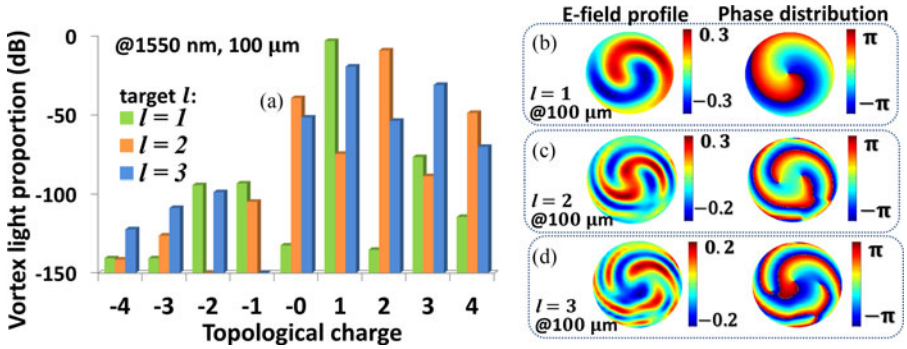

Fig. 9. (a) Proportion of vortex light with different topological charge orders after the generated vortex light propagates for 100 μm in free space; (b)–(d) the normalized electrical field profile and phase distribution of the generated vortex light at propagation distance of 100 μm. The target topological charge order is labelled as $l = 1$, 2 and 3, respectively.

proportion with other topological charge orders, which indicates good quality of the proposed generator. In Fig. 9(a) we also include the results when the target topological order is l $= 2$ and 3. In order to generate higher-order vortex light, the height of the phase disk should be increased according to Eq. 5 and it should be doubled or tripled when the target topological order is l $= 2$ or l $= 3$. When the target topological order is 2, the intensity proportion of vortex light with order of 2 is at least 30 dB larger than that of other topological charge orders. This value is lower compared with the result of the vortex light generator with target order l $= 1$. And it becomes even lower when target topological charge order is l $= 3$. The reason of this is obvious: when the height of the phase disk becomes larger for higher-order vortex light generator, the condition of the effective medium theory is difficult to be satisfied.

4. Conclusion

A fiber-based free space vortex light generator is proposed and designed based on the diffraction of the fundamental HE_{11} mode by the phase disk at the end of optical fiber. After modulated by the phase disk, the generated vortex light requires to propagate at least 100 μm in free space to get stabilized. At a propagation distance of 150 μm in free space, the Bessel beam generated vortex light has a dark central core with radius of only 3 μm, compared with 14.2 μm radius for Gaussian beam generated vortex light. The quasi-diffractionless feature of the Bessel beam generated vortex light has been demonstrated, indicating much smaller diffraction than that of the Gaussian beam generated vortex light. The performance of the vortex light generator is evaluated by FDTD simulation where the operating wavelength range, polarization sensitivity and fabrication tolerance are characterized by using the beam purity. The simulation results show our proposed free space vortex light generator has good quality and can find applications in high solution imaging, OAM communications and so on.

References

[1] J. Leach, E. Yao, and M. J. Padgett, "Observation of the vortex structure of a non-integer vortex beam," *New J. Phys.*, vol. 6, no. 1, Jul. 2004, Art. no. 71.
[2] J. F. Nye and M. V. Berry, "Dislocations in wave trains," *Philos. Trans. R. Soc. London, Ser. A*, vol. 336, no. 1605, pp. 165–190, Jan. 1974.
[3] G. Tkachenko, M. Chen, K. Dholakia, and M. Mazilu, "Is it possible to create a perfect fractional vortex beam?" *Optica*, vol. 4, no. 3, pp. 330–333, Mar. 2017.
[4] M. S. Soskin, V. N. Gorshkov, M. V. Vasnetsov, J. T. Malos, and N. R. Heckenberg, "Topological charge and angular momentum of light beams carrying optical vortices," *Phys. Rev. A*, vol. 56, no. 5, pp. 4064–4075, Nov. 1997.
[5] L. L. Li and F. Li, "Beating the Rayleigh limit: Orbital-angular-momentum-based super-resolution diffraction tomography," *Phys. Rev. E*, vol. 88, no. 3, pp. 033205-1–033205-6, Sep. 2013.

[6] K. I. Willig, J. Keller, M. Bossi, and S. W. Hell, "STED microscopy resolves nanoparticle assemblies," *New J. Phys.*, vol. 8, no. 6, pp. 106-1–106-8, Jun. 2006.
[7] L. Yan *et al.*, "Q-plate enabled spectrally diverse orbital-angular-momentum conversion for stimulated emission depletion microscopy," *Optica*, vol. 2, no. 10, pp. 900–903, Oct. 2015.
[8] J. Zhao, L. D. Chremmos, D. Song, D. N. Christodoulides, N. K. Efremidis, and Z. Chen, "Curved singular beams for three-dimensional particle manipulation," *Sci. Rep.*, vol. 5, Jul. 2015, Art. no. 12086.
[9] D. Cojoc, V. Garbin, E. Ferrari, R. Proietti, S. Cabrini, and E. Di Fabrizio, "Laser trapping and micro-manipulation using optical vortices," *Microelectron. Eng.*, vol. 78, pp. 125–131, Mar. 2005.
[10] J. Wang *et al.*, "Terabit free-space data transmission employing orbital angular momentum multiplexing," *Nature Photon.*, vol. 6, no. 7, pp. 488–496, Jun. 2012.
[11] R. J. Essiambre, R. Ryf, N. K. Fontaine, and S. Randel, "Space-division multiplexing in multimode and multicore fibers for high-capacity optical communications," *IEEE Photon. J.*, vol. 5, no. 2, Apr. 2013, Art. no. 071307.
[12] Y. Yan *et al.*, "High-capacity millimetre-wave communications with orbital angular momentum multiplexing," *Nature Commun.*, vol. 5, Sep. 2014, Art. no. 4876.
[13] H. Huang *et al.*, "100 Tbit/s free-space data link enabled by three-dimensional multiplexing of orbital angular momentum, polarization, and wavelength," *Opt. Lett.*, vol. 39, no. 2, pp. 197–200, Jan. 2014.
[14] E. Nagali *et al.*, "Quantum information transfer from spin to orbital angular momentum of photons," *Phys. Rev. Lett.*, vol. 103, no. 1, pp. 013601-1–013601-4, Jun. 2009.
[15] P. Zhang, X. F. Ren, X. B. Zou, B. H. Liu, Y. F. Huang, and G. C. Guo, "Demonstration of one-dimensional quantum random walks using orbital angular momentum of photons," *Phys. Rev. A*, vol. 75, no. 5, pp. 052310-1–052310-4, May 2007.
[16] A. E. Willner *et al.*, "Design challenges and guidelines for free-space optical communication links using orbital-angular-momentum multiplexing of multiple beams," *J. Opt.*, vol. 18, no. 7, Jun. 2016, Art. no. 074014.
[17] D. McGloin and K. Dholakia, "Bessel beams: Diffraction in a new light," *Contemp. Phys.*, vol. 46, no. 1, pp. 15–28, Jan./Feb., 2005.
[18] P. Vaity and L. Rusch, "Perfect vortex beam: Fourier transformation of a Bessel beam," *Opt. Lett.*, vol. 40, no. 4, pp. 597–600, Feb. 2015.
[19] A. M. Summers *et al.*, "Spatial characterization of Bessel-like beams for strong-field physics," *Opt. Exp.*, vol. 25, no. 3, pp. 1646–1655, Feb. 2017.
[20] T. Zhao *et al.*, "Multicolor 4D fluorescence microscopy using ultrathin bessel light sheets," *Sci. Rep.*, vol. 6, Jun. 2016, Art. no. 26159.
[21] R. M. Power and J. Huisken, "A guide to light-sheet fluorescence microscopy for multiscale imaging," *Nat. Methods*, vol. 14, no. 4, pp. 360–373, Mar. 2017.
[22] J. Arlt, V. Garces-Chavez, W. Sibbett, and K. Dholakia, "Optical micromanipulation using a Bessel light beam," *Opt. Commun.*, vol. 197, no. 4, pp. 239–245, Oct. 2001.
[23] V. Garcés-Chávez, K. Volke-Sepulveda, S. Chávez-Cerda, W. Sibbett, and K. Dholakia, "Transfer of orbital angular momentum to an optically trapped low-index particle," *Phys. Rev. A*, vol. 66, no. 6, pp. 063402-1–063402-8, Dec. 2002.
[24] V. Garcés-Chávez, D. McGloin, H. Melville, W. Sibbett, and K. Dholakia, "Simultaneous micromanipulation in multiple planes using a self-reconstructing light beam," *Nature*, vol. 419, no. 6903, pp. 145–147, Sep. 2002.
[25] K. Volke-Sepulveda, V. Garcés-Chávez, S. Chávez-Cerda, J. Arlt, and K. Dholakia, "Orbital angular momentum of a high-order Bessel light beam," *J. Opt. B Quantum Semiclassical Opt.*, vol. 4, no. 2, pp. S82–S89, Mar. 2002.
[26] J. A. Davis, E. Carcole, and D. M. Cottrell, "Nondiffracting interference patterns generated with programmable spatial light modulators," *Appl. Opt.*, vol. 35, no. 4, pp. 599–602, Feb. 1996.
[27] D. N. Schimpf, J. Schulte, W. P. Putnam, and F. X. Kärtner, "Generalizing higher-order bessel-gaussian beams: Analytical description and demonstration," *Opt. Exp.*, vol. 20, no. 24, pp. 26852–26867, Nov. 2012.
[28] A. Vasara, J. Turunen, and A. T. Friberg, "Realization of general nondiffracting beams with computer-generated holograms," *J. Opt. Soc. Amer. A*, vol. 6, no. 11, pp. 1748–1754, Nov. 1989.
[29] T. C. Choy, *Effective Medium Theory: Principles and Applications*. London, U.K.: Oxford Univ. Press, 2015.
[30] B. Zhou, F. Lei, L. Liu, and L. Wang, "All-optical-fiber orbital angular momentum mode generator with a helical phase disk inserted between fibers," *IEEE Photon. J.*, vol. 7, no. 6, Dec. 2015, Art. no. 7103408.
[31] A. W. Snyder and J. D. Love, *Optical Waveguide Theory*. Boston, MA, USA: Chapman & Hall, 1983, Sec. 13.
[32] O. Brzobohatý, T. Cižmar, and P. Zemanek, "High quality quasi-Bessel beam generated by round-tip axicon," *Opt. Exp.*, vol. 16, no. 17, pp. 12688–12700, Aug. 2008.
[33] G. Zhou, "Analytical vectorial structure of Laguerre-Gaussian beam in the far field," *Opt. Lett.*, vol. 31, no. 17, pp. 2616–2618, Sep. 2006.
[34] A. Emoto *et al.*, "Form birefringence in intrinsic birefringent media possessing a subwavelength structure," *Appl. Opt.*, vol. 49, no. 23, pp. 4355–4361, Aug. 2010.
[35] R. P. MacDonald, S. A. Boothroyd, T. Okamoto, J. Chrostowski, and B. A. Syrett, "Interboard optical data distribution by bessel beam shadowing," *Opt. Commun.*, vol. 122, nos. 4–6, pp. 169–177, Jan. 1996.